Electronic supplementary information for

Facile synthesis of electrocatalytically active Cu/graphite using the negative electrode of spent Li-ion batteries

Hiroshi Itahara*, Naonari Sakamoto, Naoko Takahashi, Satoru Kosaka and Yasuhiro Takatani

Toyota Central R&D Labs., Inc., 41-1 Yokomichi Nagakute, Aichi 480-1192, Japan
E-mail: h-itahara@mosk.tytlabs.co.jp

(1) Characteristics of S-NE sample

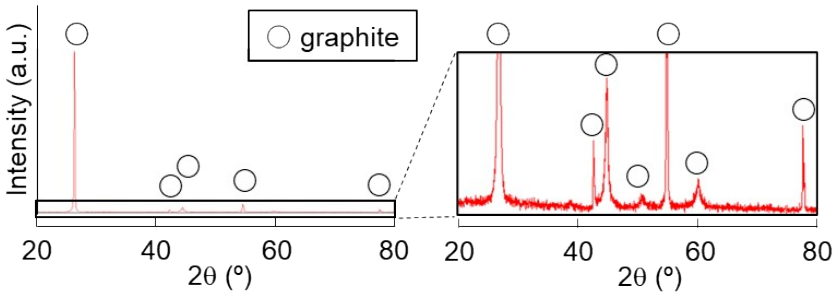

Figure S1. Powder XRD pattern for S-NE sample.

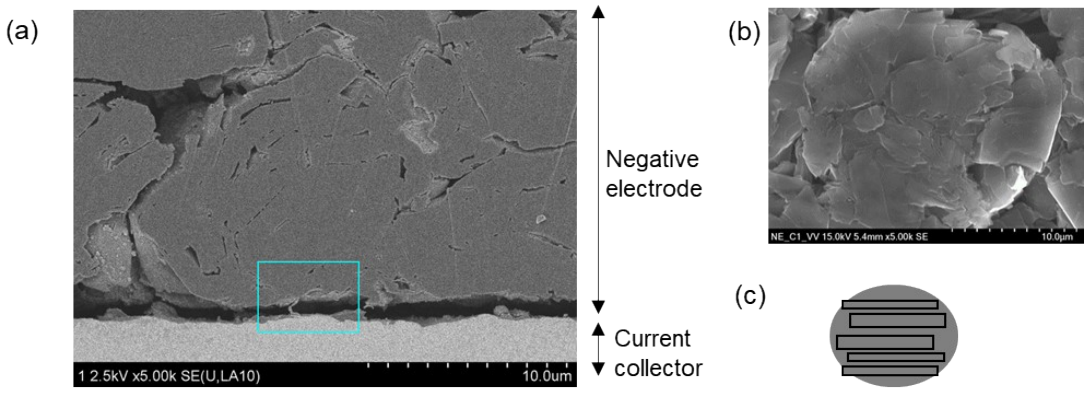

Figure S2. (a) Cross-sectional SEM image of the negative electrode layer of a spent lithium-ion battery, (b) SEM image taken for the surface of the negative electrode layer and (c) schematic representation of agglomerates of primary graphite platelets.

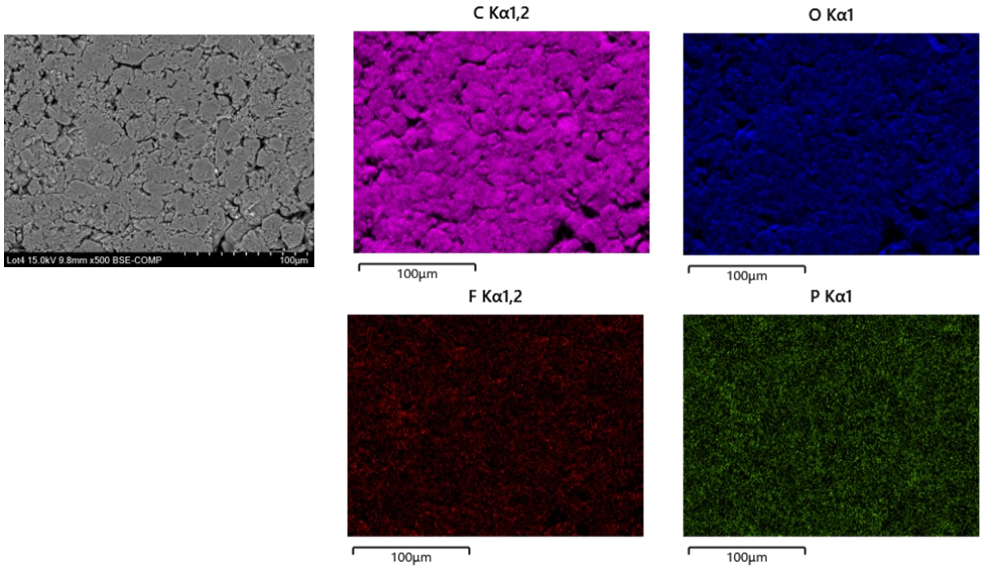

Figure S3. SEM and SEM-EDX mapping images for S-NE sample powder.

(2) Composition analysis by inductively coupled plasma mass spectrometry (ICP-MS, Agilent Technologies, Agilent 8900) and combustion ion chromatography by a combination of an automated combustion unit (Nittoseiko Analytech Co., Ltd, AQF-100) and an IC system (Thermo Fisher Scientific, ICS-1100).

Table S1. Amounts of impurities and copper loaded (wt%)

	Li	F	P	Ni	Co	Al	Cu	Cl
S-NE	1.3	1.1	0.37	2.6	0.47	0.155	0.006	0.02
W-NE	0.17	0.04	0.03	1.6	0.27	0.076	0.005	0.01
Cu-NE_RT	0.15	0.05	0.26	1.5	0.27	0.12	3.3	0.07
Cu-NE_HT450	0.16	0.07	0.17	1.6	0.28	0.17	3.4	0.06

(3) Peeling test

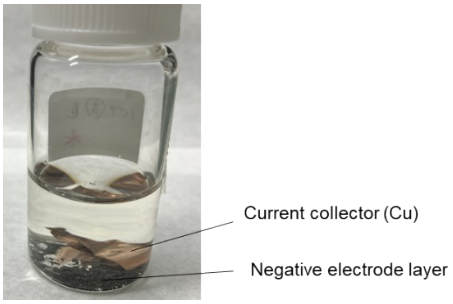

Figure S4. Photograph taken for the negative electrode immersing into water

(4) Comparison of S-NE and Cu-NE_RT samples

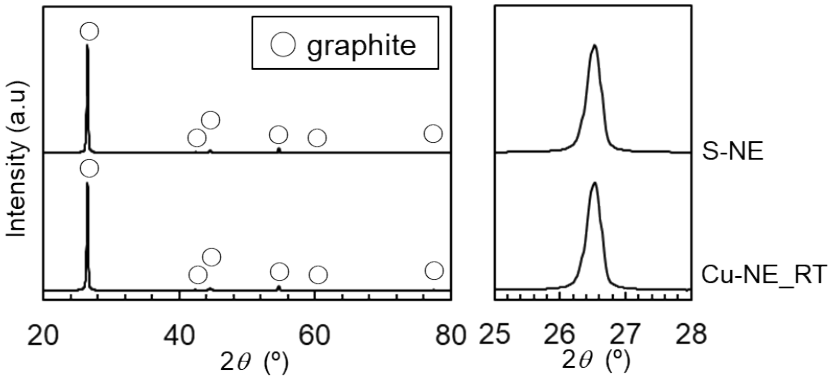

Figure S5. Powder XRD patterns for S-NE and Cu-NE_RT samples

(5) XAFS measurements for Cu-NE_RT samples

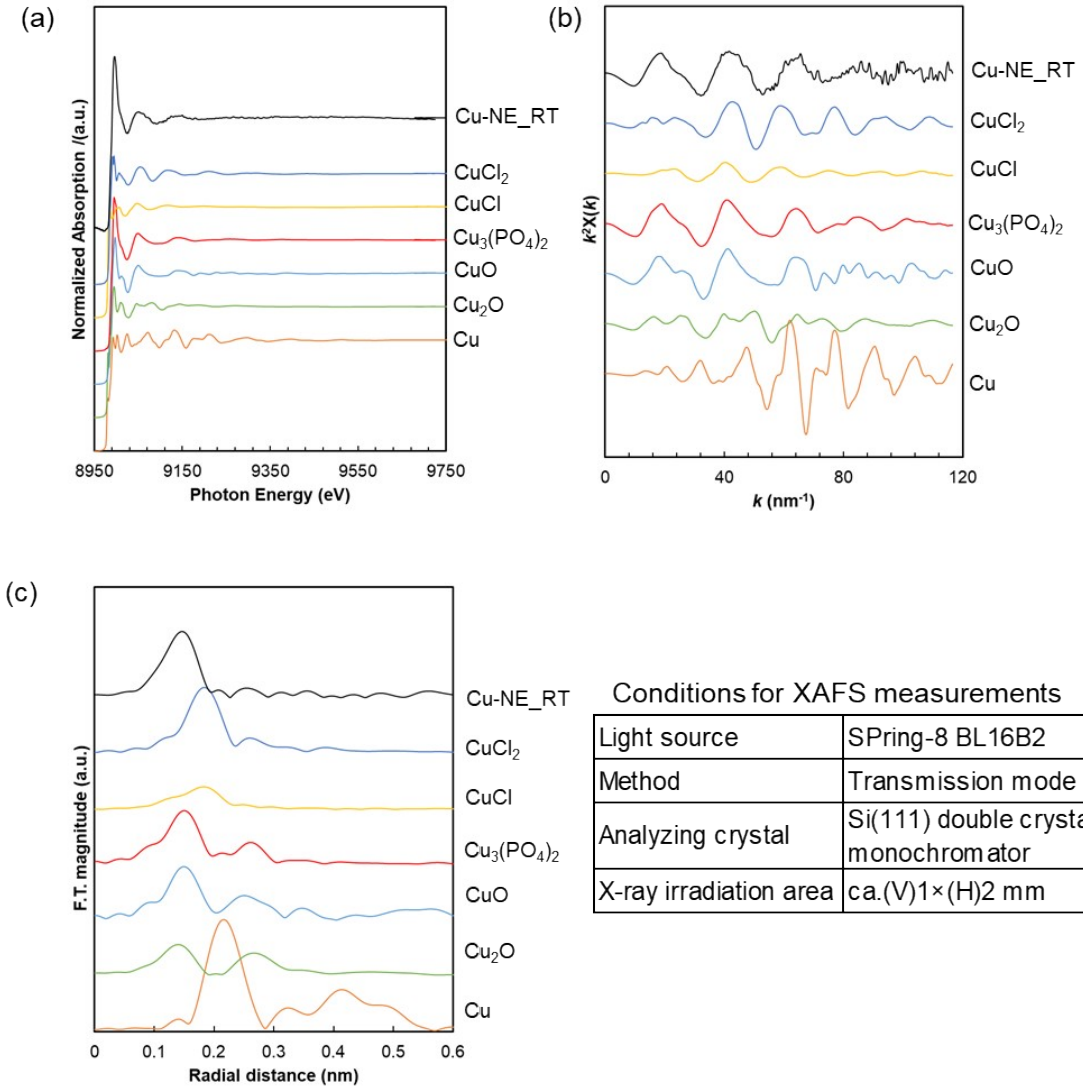

Conditions for XAFS measurements

Light source	SPring-8 BL16B2
Method	Transmission mode
Analyzing crystal	Si(111) double crystal monochromator
X-ray irradiation area	ca.(V)1×(H)2 mm

Figure S6. (a) Cu K-edge X-ray absorption spectra for Cu-NE_RT and reference (metallic Cu and copper oxides) samples. (b) k2-weighted oscillations extracted from the Cu K-edge extended X-ray absorption fine structure spectra as functions of the wave vector. (c) Fourier transforms derived from the oscillations. The range of the Fourier transformation is k = 30–100 nm^{-1}.

(6) Raman spectrum

Ex situ Raman spectroscopy was performed using an excitation laser with a wavelength of 532 nm and a laser Raman microscope (Nanophoton Corp., RAMANtouch). The intensity of the laser beam was approximately 0.3 mW, the exposure time was 2 s, and the acquisition time for a Raman spectrum was 20 s.

Integrated intensity ratio

	S-NE	W-NE	Cu-NE_RT
I_D/I_G	0.249	0.212	0.217

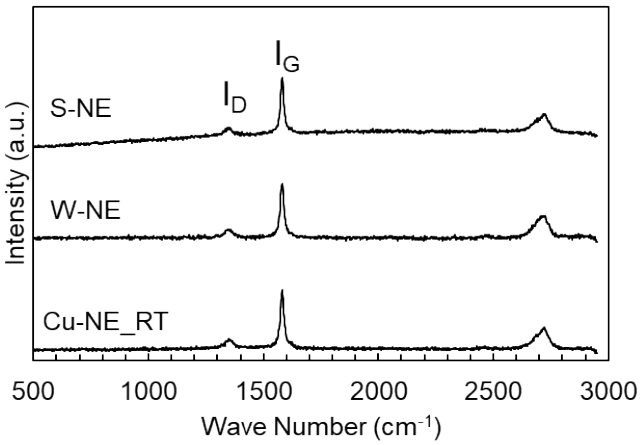

Figure S7. Raman spectra for S-NE, W-NE and Cu-NE_RT samples.

(7) Microstructural analysis for reference samples

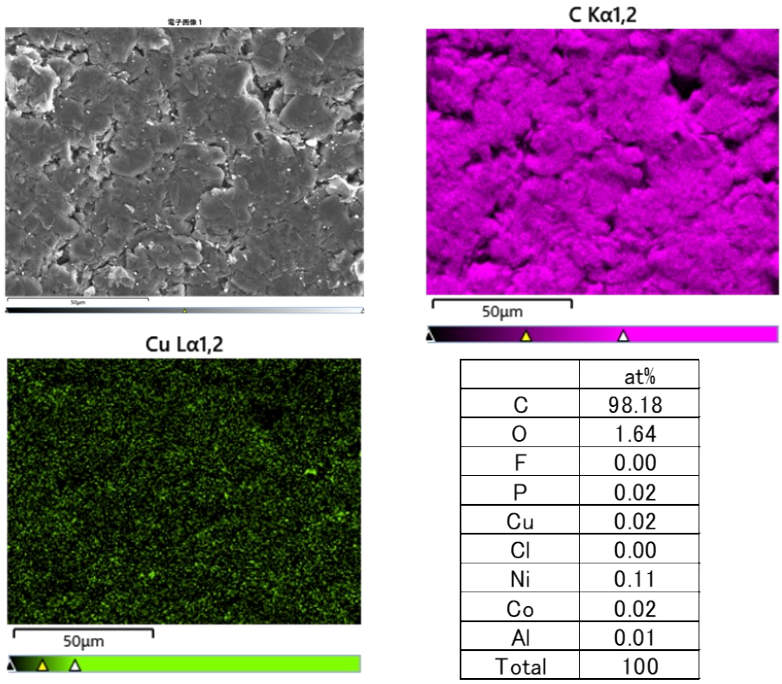

	at%
C	98.18
O	1.64
F	0.00
P	0.02
Cu	0.02
Cl	0.00
Ni	0.11
Co	0.02
Al	0.01
Total	100

Figure S8. SEM and SEM-EDX mapping images for the sample prepared by dispersing W-NE powder into $CuCl_2$ aqueous solution.

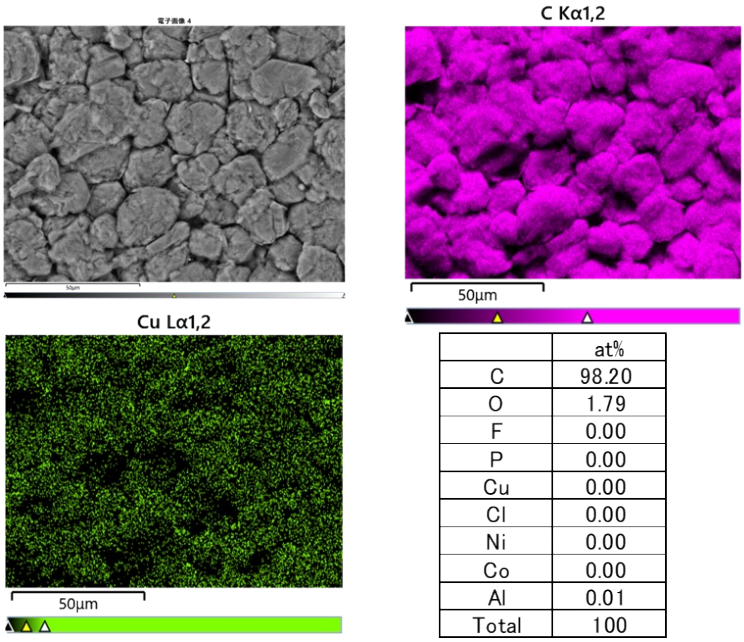

	at%
C	98.20
O	1.79
F	0.00
P	0.00
Cu	0.00
Cl	0.00
Ni	0.00
Co	0.00
Al	0.01
Total	100

Figure S9. SEM and SEM-EDX mapping images for the sample prepared by dispersing pristine graphite powder (commercial powder, OMAC) into $CuCl_2$ aqueous solution.

(8) Microstructural analysis for Ni-NE, Co-NE and Fe-NE_RT samples

Fe-NE, Co-NE and Ni-NE_RT samples were prepared in the same process for the Cu-NE_RT sample. S-NE powder (250 mg) was dispersed into a MCl_2 aqueous solution (M=Fe, Co or Ni, 7.4 mM, 100 mL) and ultrasonicated for 15 min at room temperature; the product was collected by filtration and dried under vacuum at 80 °C for 2 h.

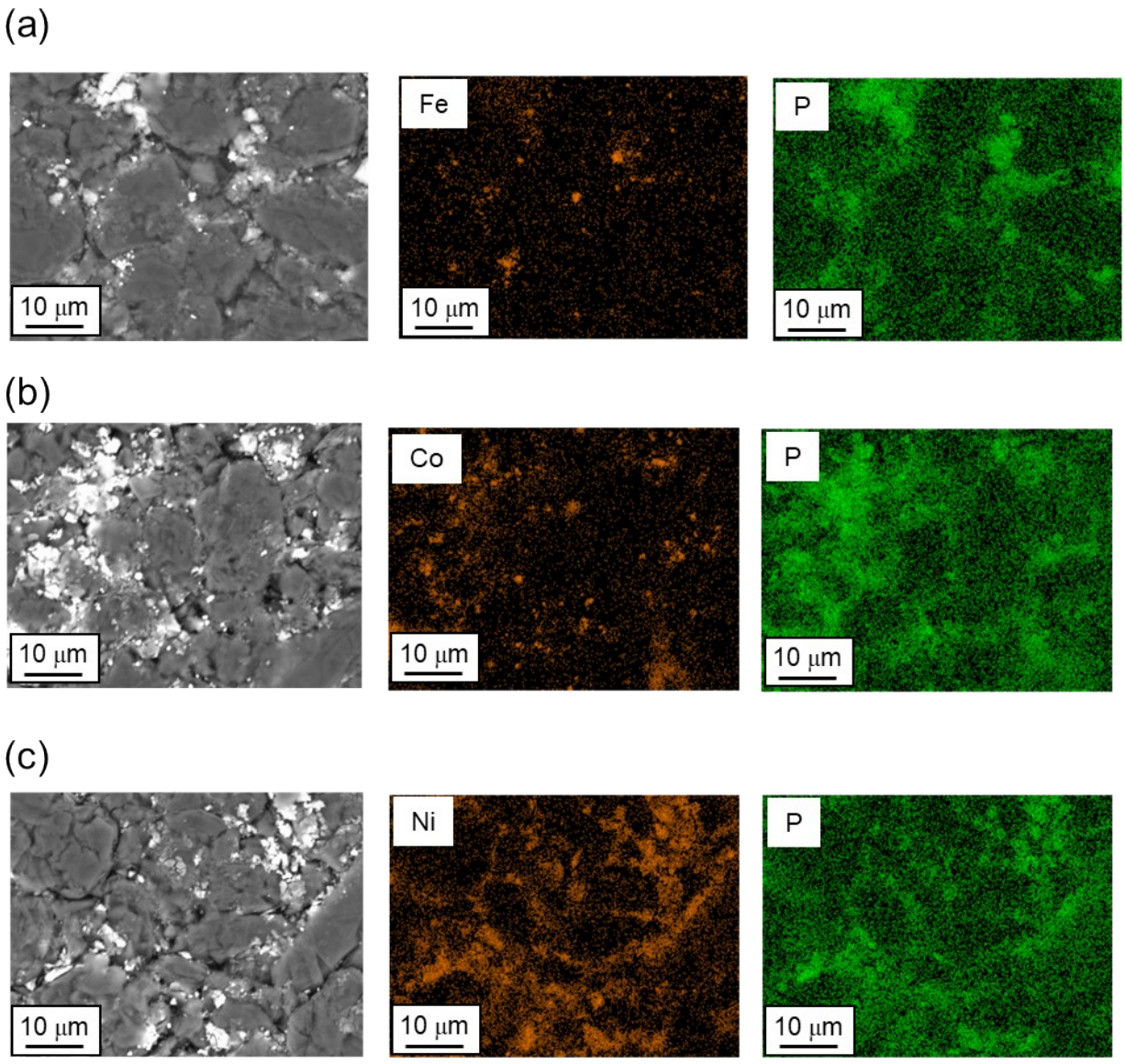

Figure S10. SEM and SEM-EDX mapping images for (a) Fe-NE, (b) Co-NE and (c) Ni-NE_RT samples.

(9) Microstructural analysis for Cu-NE_RT sample

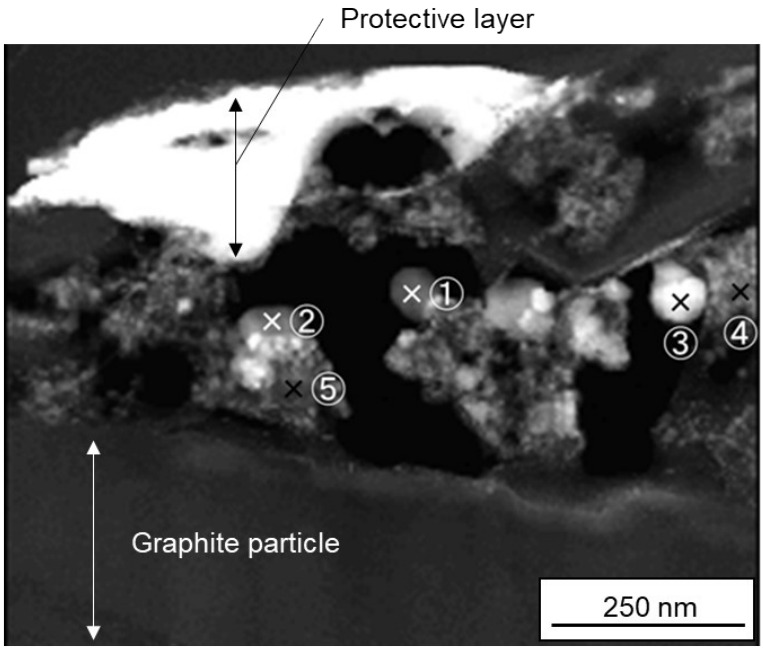

at%

	①	②	③	④	⑤
C	19.71	22.70	19.73	57.19	56.79
Cu	75.84	73.36	74.38	22.54	21.85
O	0.56	1.50	2.06	14.11	14.63
P	1.13	0.58	0.71	5.40	5.55
F	2.02	1.59	2.56	___	___
Cl	0.05	___	0.24	0.63	1.09
Ni	___	0.11	0.12	0.03	0.04
Co	0.02	0.16	0.11	0.11	___
Al	0.66	___	0.09	___	0.05
	100	100	100	100	100
P/Cu	0.01	0.01	0.01	0.24	0.25
O/Cu	0.01	0.02	0.03	0.63	0.67

Figure S11. Cross-sectional STEM image for Cu-NE_RT sample.

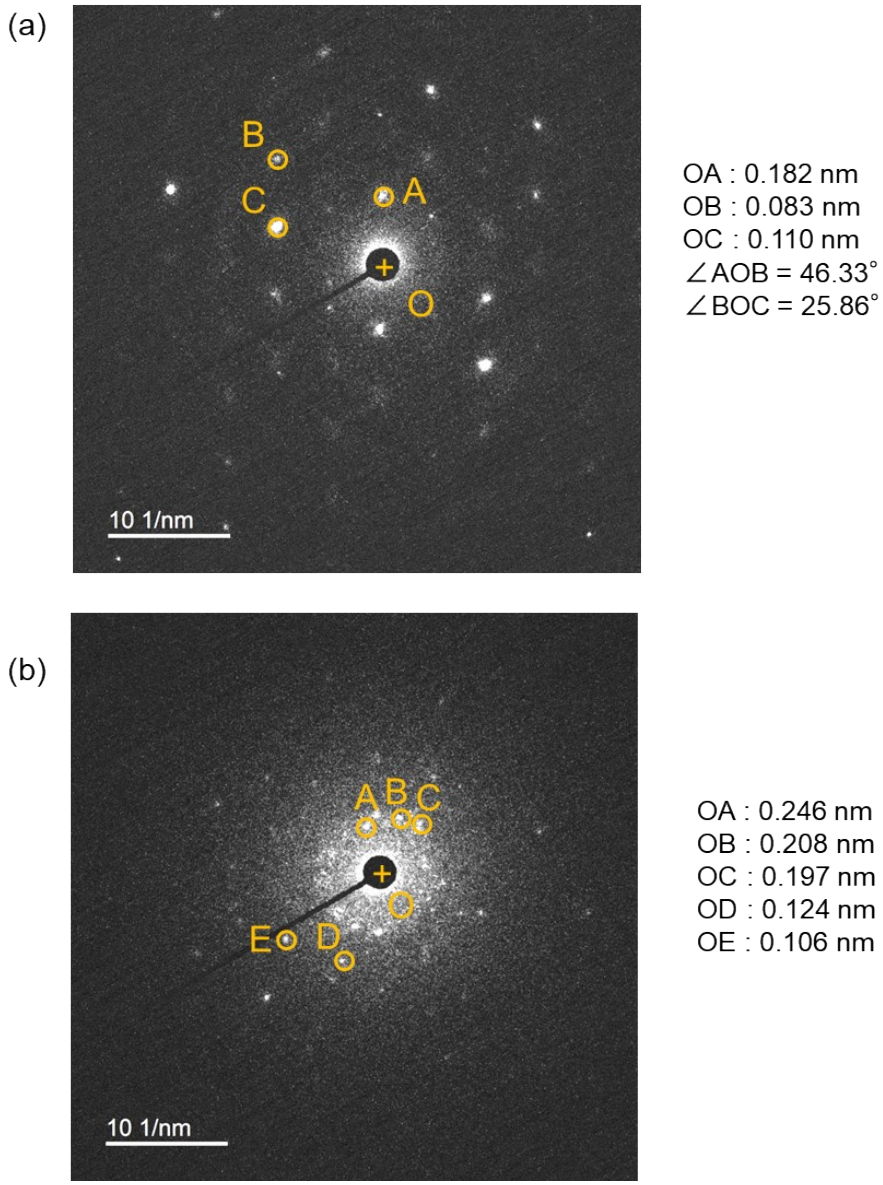

Figure S12. Nano beam diffraction patterns for (a) position No.1 and (b) position No.4 in Fig.S10.

(10)XAFS measurements for Cu-NE_RT and Cu-NE_HT samples

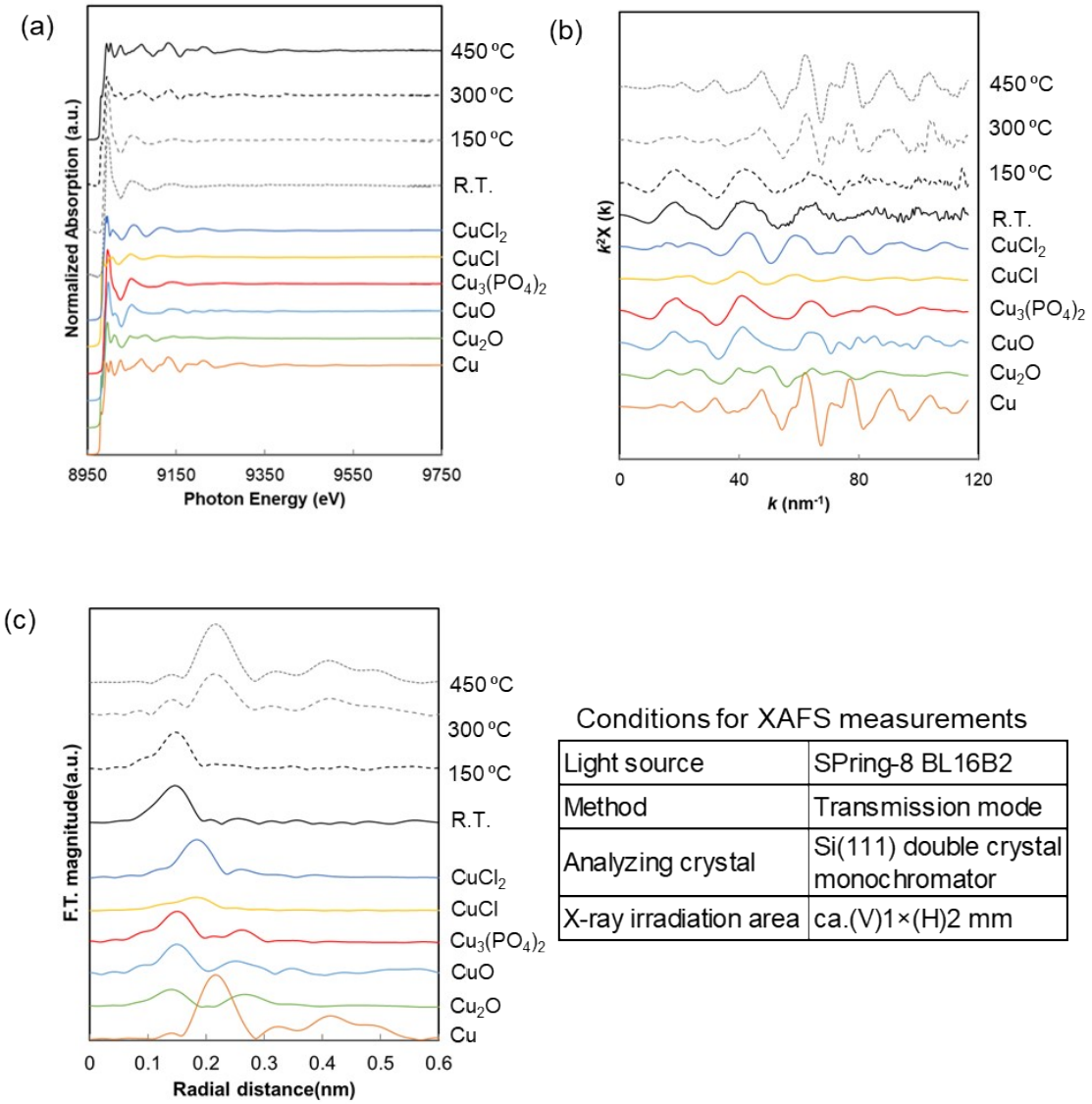

Conditions for XAFS measurements

Light source	SPring-8 BL16B2
Method	Transmission mode
Analyzing crystal	Si(111) double crystal monochromator
X-ray irradiation area	ca.(V)1×(H)2 mm

Figure S13. (a) Cu K-edge X-ray absorption spectra for Cu-NE_RT, Cu-NE_HT and reference (metallic Cu and copper oxides) samples. (b) k2-weighted oscillations extracted from the Cu K-edge extended X-ray absorption fine structure spectra as functions of the wave vector. (c)Fourier transforms derived from the oscillations. The range of the Fourier transformation is k = 30–100 nm^{-1}.

(11) Characteristics of the reference Cu-Gr_imp and Cu-Gr_mix samples

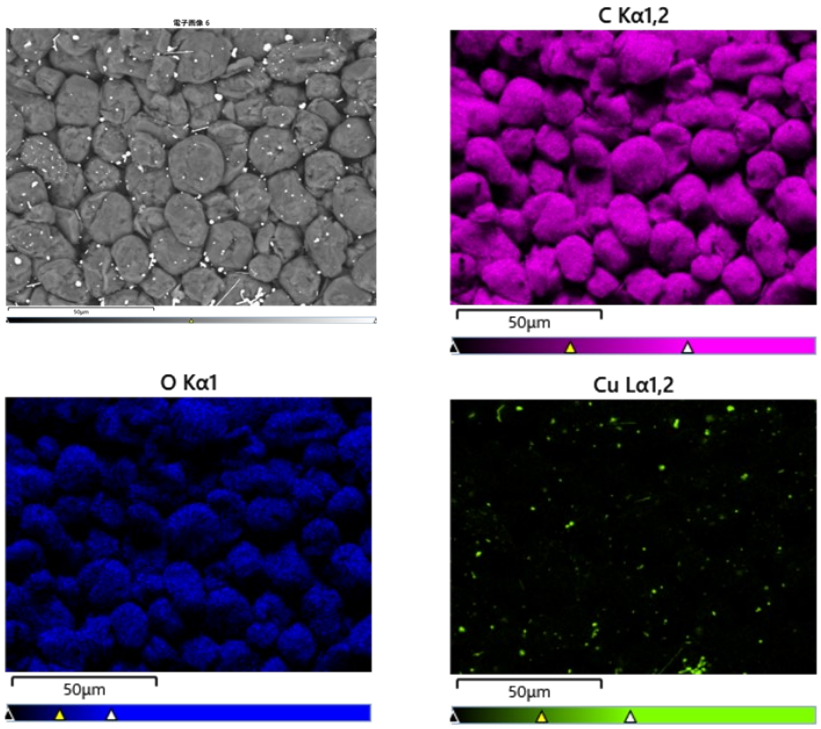

Figure S14. SEM image and SEM-EDX mapping images for Cu-Gr_imp sample.

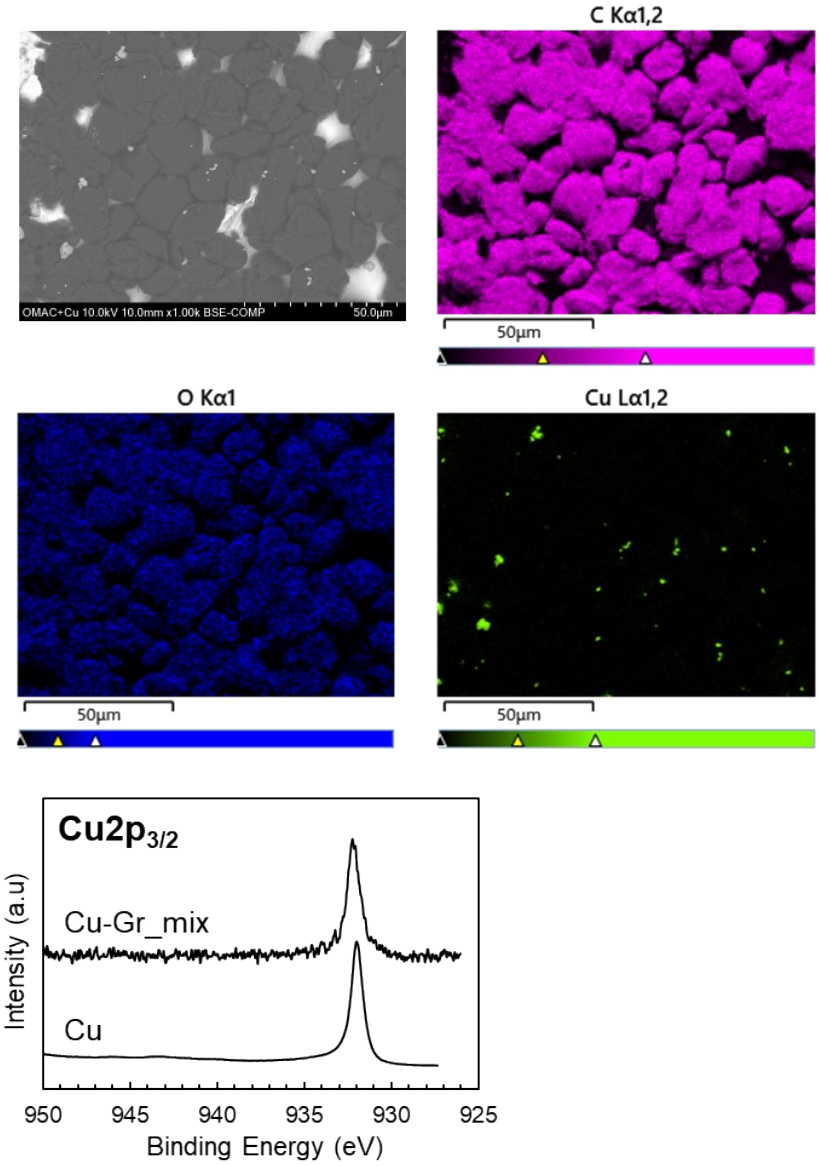

Conditions for HAXPES measurements

Light source	SPring-8 BL16XU
Photon energy	7.942 keV
Take off angle	80°
X-ray irradiation area	ca.(V)40×(H)350 μm

Figure S15. SEM image, SEM-EDX mapping images and HAXPES spectrum for Cu-Gr_mix sample (Cu: commercial sample).

(12) Microstructural analysis for Cu-NE_ECT sample

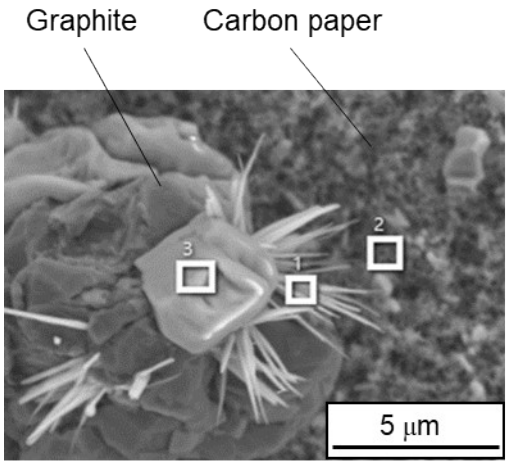

at%

	1	2	3
C	25.61	78.16	13.19
Cu	21.52	1.18	1.14
O	26.48	2.39	41.96
P	0.15	0	0.13
F	2.09	10.91	0.30
Cl	0	0	0
Ni	0	0.8	0.47
Co	0	0.92	0.52
Al	0.06	0	0.05
K	24.09	5.65	42.24
Total	100	100	100

Figure S16. SEM images and SEM-EDX data for Cu-NE_ECT sample.

(13) Dissolved amount of Cu in anolyte solution

Dissolved amount of Cu in anolyte after electrochemical treatment (ECT) by using inductively coupled plasma mass spectrometry (ICP-MS, Agilent Technologies, Agilent 8900).

Table S2. Dissolved amount of Cu in anolyte (μg/ml)

Cu-NE_ETC	0.35
NE_HT450	0.12
Cu_Gr_mix	0.32

(14) Characteristics of Cu-NE_HT450 sample after electrochemical measurements

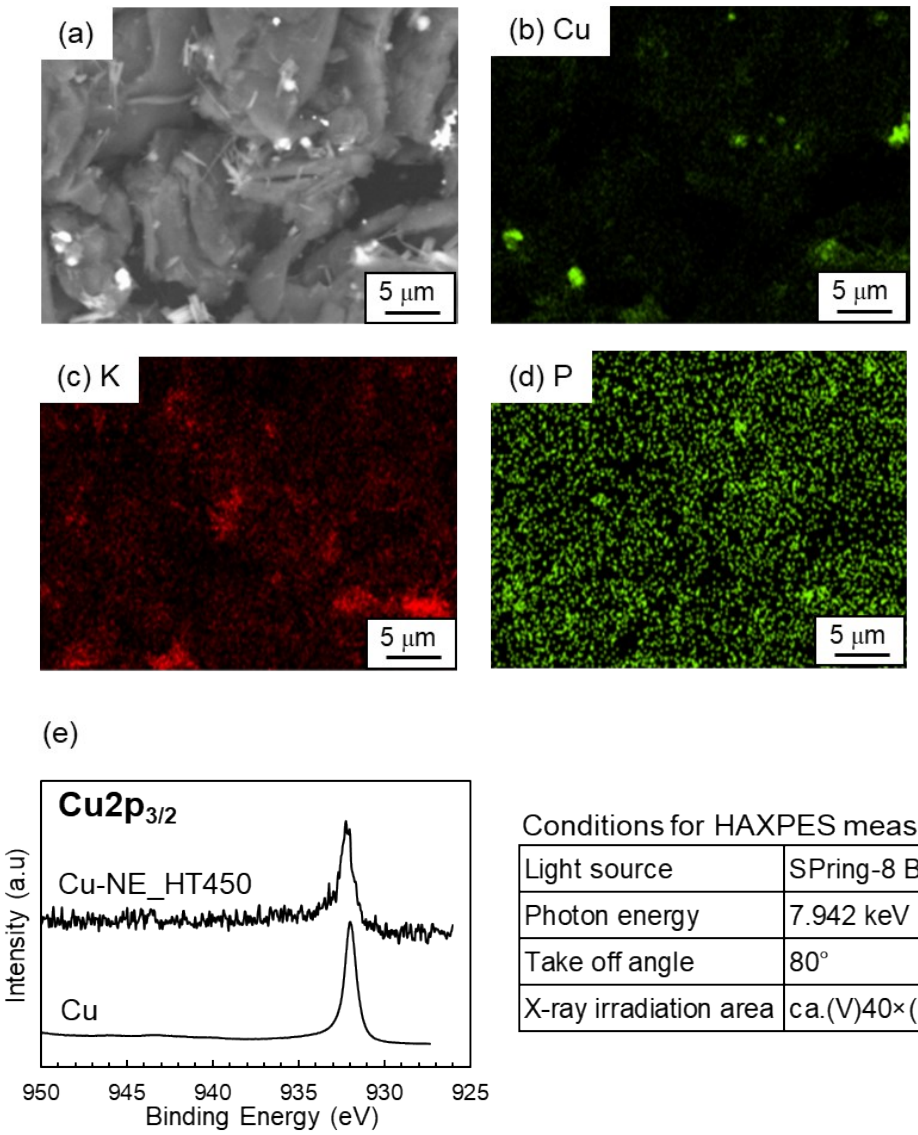

Conditions for HAXPES measurements

Light source	SPring-8 BL16XU
Photon energy	7.942 keV
Take off angle	80°
X-ray irradiation area	ca.(V)40×(H)350 μm

Figure S17. (a) SEM image, (b)-(d) SEM-EDX mapping images and (e) HAXPES spectrum for Cu-NE_HT450 sample after electrochemical measurements (Cu in (d): commercial sample).

(15) Characteristics of Cu-Gr_mix sample after electrochemical measurements

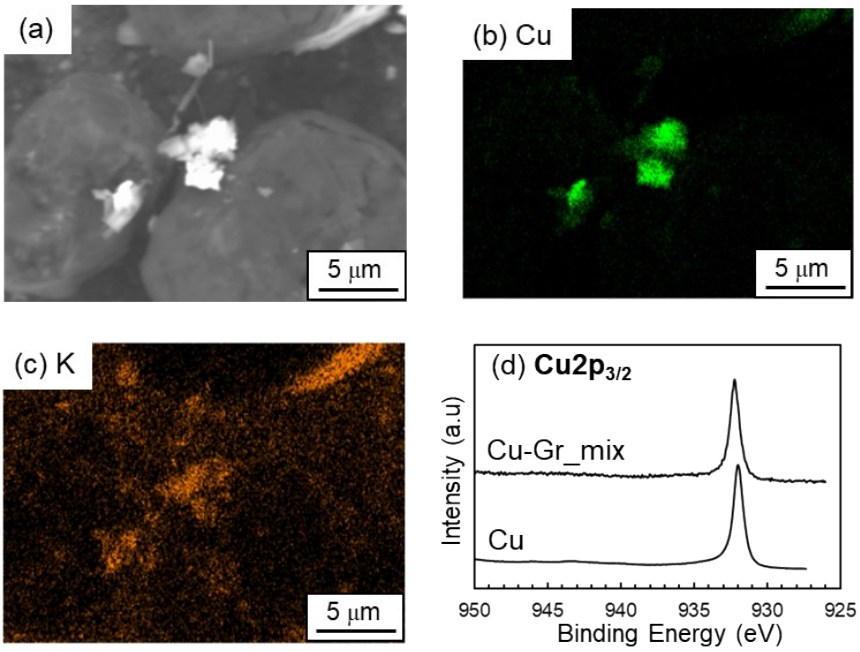

Conditions for HAXPES measurements

Light source	SPring-8 BL16XU
Photon energy	7.942 keV
Take off angle	80°
X-ray irradiation area	ca.(V)40×(H)350 μm

Figure S18. (a) SEM image, (b),(c) SEM-EDX mapping images and (d) HAXPES spectrum for Cu-Gr_mix sample after electrochemical measurements (Cu in (d): commercial sample).

(16) Electrochemical properties for S-NE and W-NE samples

Electrical flow and gas generation were observed during electrochemical measurements. The measurement conditions are described in the main text.

Current efficiency is defined as follows:

Current efficiency (%) = (mole number × electron number) / (total charge / Faraday constant) × 100

Here, the molar number of each product was calculated using the amount measured and the molar weight. The electron number required to produce CO, CH_4, C_2H_4 are 2, 8 and 12, respectively.

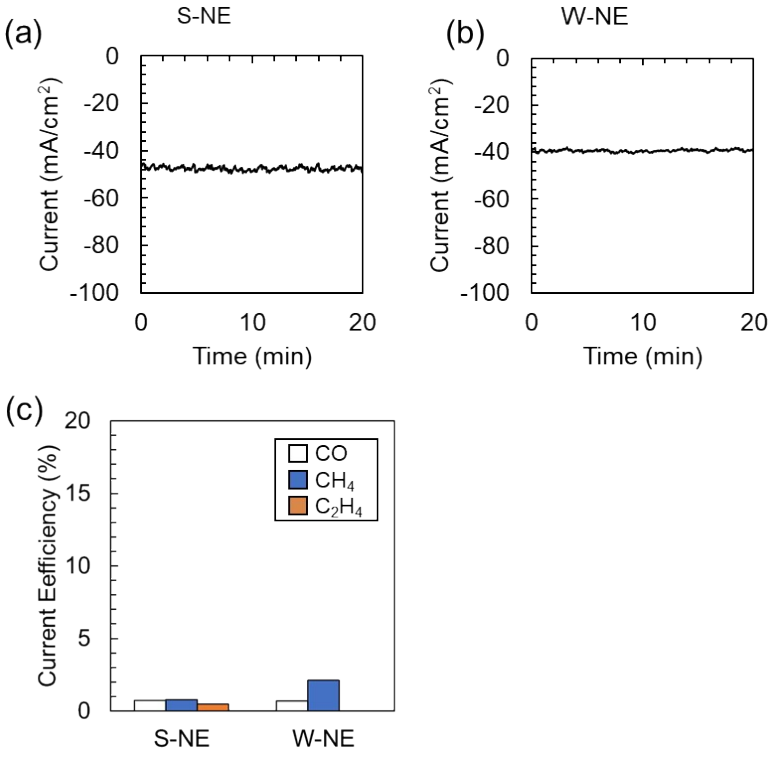

Figure S19. (a),(b) current density change on time and (c) current efficiency for production of CO, CH_4 and C_2H_4 for S-NE and W-NE samples.

(17) Electrochemical properties for Cu-NE_ETC, Cu-NE_HT450 and Cu-Gr_mix samples

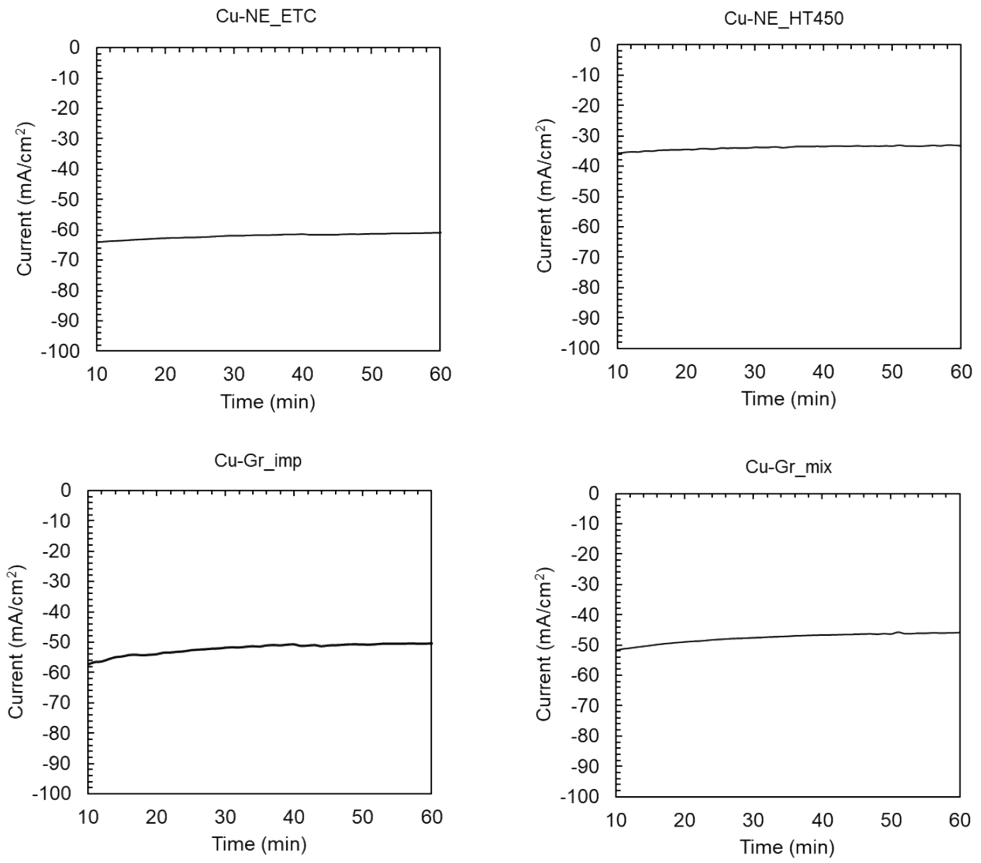

Figure S20. Current density change on time for Cu-NE_ETC, Cu-NE_HT450, Cu-Gr_imp and Cu-Gr_mix samples.

Table.S3 Current efficiencies of C_1 (CO, CH_4 and formic acid) and C_{2+} (C_2H_4, ethanol and propanol), and the C_{2+}/C_1 ratio.

	H_2	CH_4	CO	HCOOH	C_2H_4	EtOH	PrOH	C_{2+}/C_1
Cu-NE_ETC	59.1	3.72	0.00	1.00	3.58	3.57	0.81	1.69
Cu-NE_HT450	80.7	0.90	0.54	0.30	2.92	1.40	0.55	2.81
Cu-Gr_imp	86.0	0.27	0.48	1.67	0.12	0.77	0.53	0.58
Cu_Gr_mix	50.6	7.50	3.14	2.06	6.20	3.94	0.72	0.86

(18) Characteristics of commercial Cu powder before and after electrochemical measurements

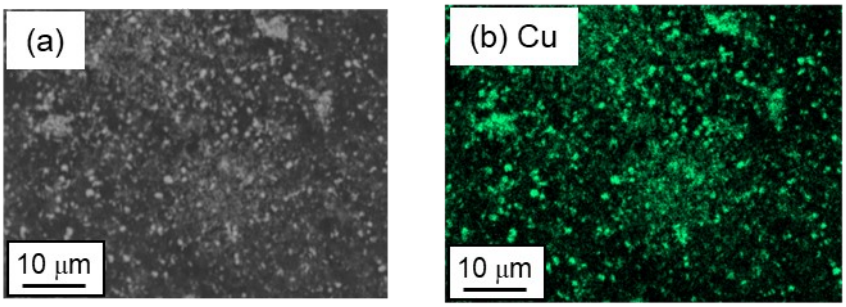

Figure S21. (a) SEM image and (b) SEM-EDX mapping image of commercial Cu powder which were taken for Cu powder loaded on carbon paper after electrochemical measurements.
.

(19) Characteristics of CuO powder before and after electrochemical measurements

CuO powder was prepared using the spent negative electrode composed of a graphite electrode layer and a copper current-collector substrate in the same manner as previously reported[1)]. The electrode was placed in a alumina crucible and heat treated at 650 °C for 3 h in air atmosphere (Heating rate of 5°C /min). The heat-treated product was ground evenly using a mortar and a pestle.

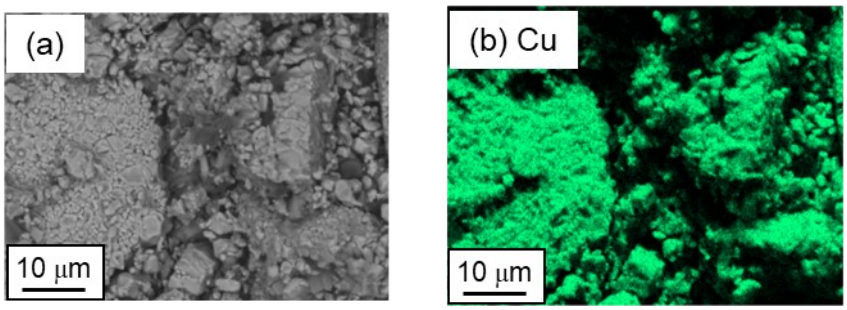

Figure S22. (a) SEM image and (b) SEM-EDX mapping image of commercial CuO powder which were taken for CuO powder loaded on carbon paper after electrochemical measurements.

(20) Electrochemical properties for commercial Cu powder and CuO samples

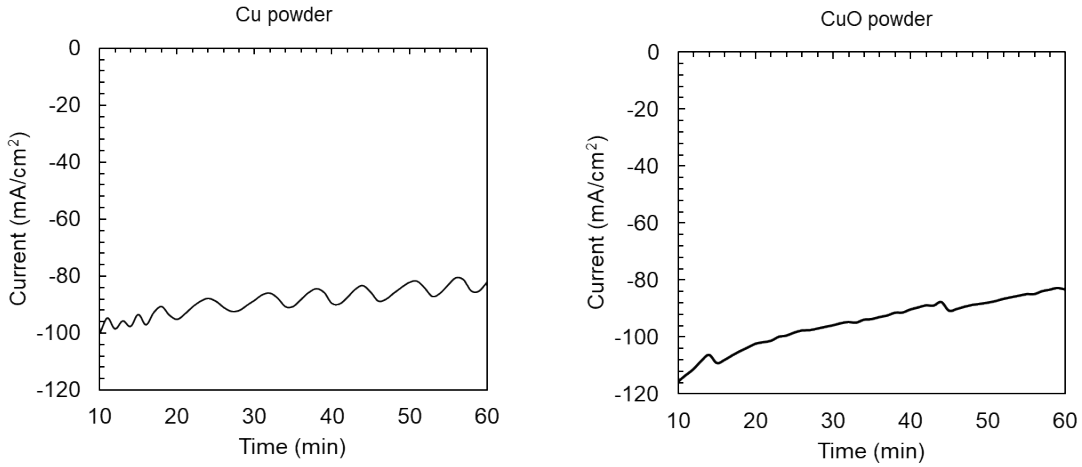

Figure S23. (a)-(c) Current density change on time for Cu powder and CuO samples.

Table.S4 Current efficiencies of C_1 (CO, CH_4 and formic acid) and C_{2+} (C_2H_4, ethanol and propanol), and the C_{2+}/C_1 ratio.

	H_2	CH_4	CO	HCOOH	C_2H_4	EtOH	PrOH	C_{2+}/C_1
Cu powder	39.3	2.40	3.48	0.44	29.5	8.20	4.59	6.70
CuO powder	66.6	1.01	0.94	0.69	10.0	3.78	1.10	5.65

(21) Comparison of the amount of the formed products.

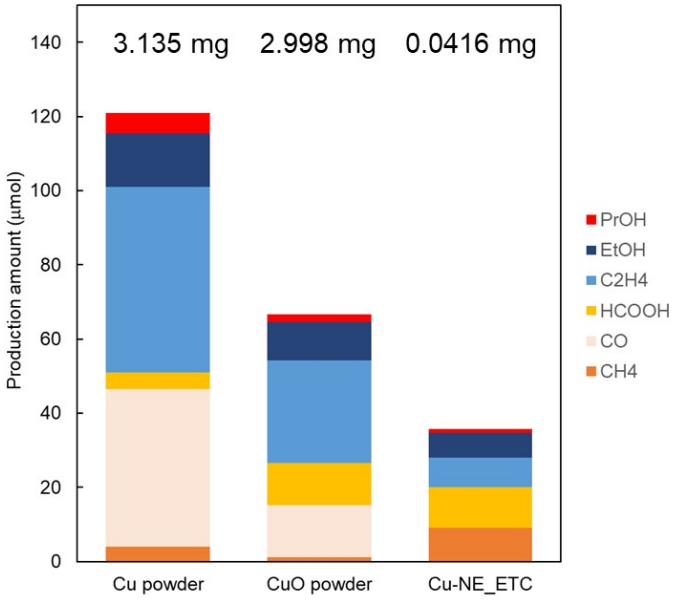

Figure S24. Comparison of the amount of the formed products. Cu amounts were 3.135 and 2.998 0.0416mg for commercial Cu powder and CuO powder, respectively. For Cu-NE_ECT sample, Cu of ~ 0.04 mg were mixed with ~1.2 mg graphite powder.

(22) Electrochemical properties for Cu nanoparticles supported graphite (nanoCu-Gr_mix sample)

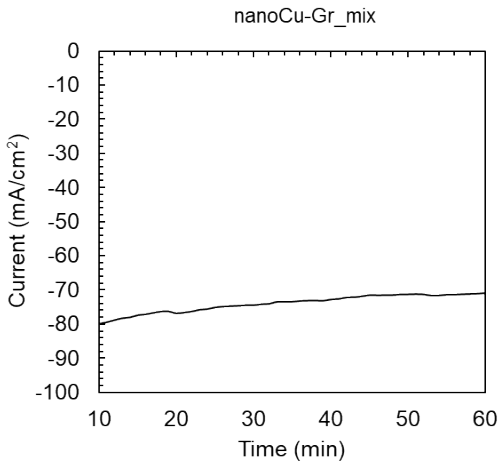

Figure S25. Current density change on time for nanoCu-Gr_mix sample.

Table.S5 Current efficiencies of C_1 (CO, CH_4 and formic acid) and C_{2+} (C_2H_4, ethanol and propanol), and the C_{2+}/C_1 ratio.

	H_2	CH_4	CO	HCOOH	C_2H_4	EtOH	PrOH	C_{2+}/C_1
nanoCu-Gr_mix	41.9	4.53	1.40	5.27	28.0	3.62	1.07	2.91

Reference

(1) Y. Zhao, H. Wang, X. Li, X. Yuan and X. Chen, Recovery of CuO/C catalyst from spent anode material in battery to activate peroxymonosulfate for refractory organic contaminants degradation", *J. Hazardous Mater.*, 2021, **420**, 126552.